Strojniški vestnik - Journal of Mechanical Engineering 54(2008)2, 81-93
UDK - UDC 537.3
Paper received: 3.1.2008
Paper accepted: 12.3.2008

Flow Analysis Through the Centrifugal Impeller of a Vacuum Cleaner Unit

Janez Rihtaršič* - Matjaž Šubelj - Marko Hočevar - Jože Duhovnik
University of Ljubljana, Faculty of Mechanical Engineering, Slovenia

Flow through the centrifugal impeller of a vacuum cleaner unit was investigated. This was done using experimental measurements and numerical simulations. Two different operational points were selected for the experiment.

Experiments were performed using flow visualization with the use of the passive seeding particles. The rotational speed was reduced by using the theory of dynamical similarity where water was used as a flow medium instead of air. Numerical simulations were performed by using compressible and incompressible fluids. Flow through impeller channels is presented as particle trajectories and relative velocities for experimental approach and as flow streamlines and relative velocities for numerical approach.

Keywords: flow visualization, centrifugal impeller, dynamical similarity, numerical simulations

0 INTRODUCTION

Aerodynamic geometry of vacuum cleaner units is a result of compromise between diverse working conditions; from high volume flow to minimum volume flow caused by full dust bag or clogged filters. Wrong geometry results in unsatisfactory performance, increased noise and surge or stall effects. To achieve a wide area of optimum operational conditions of the vacuum cleaner, it is necessary to know and understand the properties of the fluid flow at all operation conditions. This is possible to achieve through experimental measurements and/or with numerical analysis.

Numerical simulations of flow are often and successfully used for the flow visualization and flow analysis, meanwhile experimental visualizations are less frequently conducted. However, both approaches supplement each other and they are indispensably needed to understand some of the phenomena. In these cases, experimentally gathered data are used as boundary conditions for numerical simulations and sometimes, especially outside of the optimum working conditions, experimental data are sometimes the only source of information.

There are many different methods of experimental flow visualization. Some use smoke or coloured fluid other use solid additives such as small particles [1] to [5].

Two different methods of experimental flow visualization with the use of solid particles are presented in references [1] and [2]. Experimental visualization of flow through centrifugal impeller was described by Pedersen and Jacobsen [1], where Particle Image Velocimetry (PIV) method was used. They performed measurements at nominal flow and at one fourth of the nominal flow. They noticed that at operation in nominal conditions, flow follows the blade curvature without separations, whereas at operation at one fourth of the nominal flow, separations of the flow from the suction side of the blades were observed. Another approach to experimentally visualize the flow through the impeller is by capturing trajectories of the seeding particles. Such method was applied in Irabu et al. [2], where polystyrene particles were used to visualize the flow through the volute. The lather method was also used for visualization of flow through impeller at two different working conditions.

1 DYNAMICAL SIMILARITY OF THE FLOW

Application of the visualization technique to capture trajectories of the individual particles dictated the reduction of flow velocities in the centrifugal rotor. On the basis of the theory of flow similarity, this was achieved using water as a flow medium. In the follow-up, we will discuss the

*Corr. Author's Address: University of Ljubljana, Faculty of Mechanical Engineering, Aškerčeva 6, SI-1000 Ljubljana, Slovenia, janez.rihtarsic@lecad.uni-lj.si

geometrical and dynamical similarity and the selection of the measurement point.

Similarity of flows is achieved by assuring the geometrical similarity where we assume that the losses through the impeller are not dependent upon the magnitude of the flow (one impeller is a true geometrical scale of the other) and with assurance of the dynamical similarity [6] and [7]. To fulfill the requirements of the dynamical similarity, test conditions should be chosen to satisfy the Reynolds, Euler, Thoma, Froude and Weber similarity numbers, however this is usually impossible. Thoma, Froude and Weber similarity numbers deal with cavitation. Here, such conditions were selected that no cavitation occurred in all operational points and thus these numbers were not considered. The Reynolds and Euler similarity numbers are explained later.

Flow through two geometrically similar impellers is equal if the velocity fields of both flows are identical. We used the identical impeller for measurements as it is used in the vacuum cleaner unit (Fig. 2), thus the geometrical similarity was assured. By fulfilling dynamical similarity and with similarity of the Reynolds number, we can expect development of similar boundary layers and separations of the flow, as they appear with the use of air as a flow medium. Compressibility conditions were not satisfied but their influence on stream lines and relative velocities was estimated to be low. This was found by comparing CFD simulations where compressible and incompressible flows were compared (chapters 4.1.2 and 4.2.2).

When operating in the same flow medium at two different rotational speeds, the ratio of the volume flows is proportional to the ratio of the rotational speeds and the ratio of the static pressures is proportional to the square ratio of the rotational speeds. Ratio of the static pressures is also proportional to the ratio of the densities of the flow medium if the rotational speed is constant [8]:

$$\frac{Q_{a2}}{Q_{a1}} = \frac{n_{a2}}{n_{a1}} \rightarrow Q_{a1} = \frac{n_{a1}}{n_{a2}} \cdot Q_{a2} \qquad (1)$$

$$\frac{p_{a2}}{p_{a1}} = \left(\frac{n_{a2}}{n_{a1}}\right)^2 \rightarrow n_{a2} = \sqrt{\frac{p_{a2}}{p_{a1}} \cdot n_{a1}^2} \qquad (2)$$

$$\frac{p_{a2}}{p_w} = \frac{\rho_a}{\rho_w} \rightarrow p_w = \frac{\rho_w}{\rho_a} \cdot p_{a2} \qquad (3)$$

n	[min^{-1}]	rotational speed,
p	[Pa]	static pressure,
ρ	[kg/m^3]	flow medium density,
a		air flow medium index,
w		water flow medium index.

From Equations (1) to (3), we get dependence between rotational speed, when the flow medium is air, and rotational speed, when the flow medium is water (Eq. 4):

$$n_w = n_{a2} = \sqrt{\frac{p_w}{p_{a1}} \cdot \frac{\rho_a}{\rho_w} \cdot n_{a1}^2} \qquad (4).$$

Because we used identical impeller for both flow medium, the change in Reynolds number, depends only upon the change of rotational speed and upon the change of the kinematic viscosity. Relation between rotational speeds and viscosities is given in:

$$\frac{n_{a1}}{\nu_{a1}} = \frac{n_w}{\nu_w} \rightarrow \nu_{w2} = \nu_{a1} \frac{n_w}{n_{a1}} \qquad (5)$$

ν	[mm^2/s]	kinematic viscosity.

Using water as a working medium, we were able to adjust Reynolds number by changing the water temperature. However, due to the selection of the test rig materials and due to capturing frequency of the CCD camera, we were not able to achieve the same Reynolds number as when using air as a flow medium. We heated the water to 60° C. This way, we were able to obtain similarity of Reynolds number of around 31% for both volume flows.

Euler number was fulfilled because the measurement conditions were selected in accordance to the Equation (4).

2 CFD MODEL

Numerical analysis was conducted with commercial code CFX 5.7 by Ansys Inc. It is a 3-dimensional unstructured mesh code that solves a set of Reynolds-averaged Navier-Stokes equations (RANS) [9]. In the RANS approach, the mass and the momentum conservation equations together with the equations of the turbulence model form a closed set of equations. The mass conservation equation reads:

$$\frac{\partial \rho}{\partial t} + \frac{\partial}{\partial x_j}\left(\rho u_j\right) = 0 \qquad (6).$$

Here ρ is the density of the fluid and u is velocity of the fluid. The momentum conservation equation is:

$$\frac{\partial}{\partial t}(\rho u_i)+\frac{\partial}{\partial x_j}(\rho u_j u_i)=-\frac{\partial P}{\partial x_i}+\frac{\partial}{\partial x_j}\left[\mu_{eff}\left(\frac{\partial u_i}{\partial x_j}+\frac{\partial u_j}{\partial x_i}\right)\right] \quad (7),$$

where P denotes modified pressure and μ denotes viscosity.

$$\mu_{eff}=\mu+\mu_t$$

The closure of the set of the equations is simplified to the determination of the turbulent viscosity μ_t, which is usually determined by introducing the equations of the turbulence model. For this case, a two equation k-ε turbulence model was applied [9] and [10]. Additional equations read:

$$\frac{\partial(\rho k)}{\partial t}+\frac{\partial(\rho k u_j)}{\partial x_j}=\frac{\partial}{\partial x_j}\left[\left(\mu+\frac{\mu_t}{\sigma_k}\right)\frac{\partial k}{\partial x_j}\right]+P_k-\rho\varepsilon \quad (8)$$

and

$$\frac{\partial(\rho\varepsilon)}{\partial t}+\frac{\partial(\rho\varepsilon u_j)}{\partial x_j}=\frac{\partial}{\partial x_j}\left[\left(\mu+\frac{\mu_t}{\sigma_\varepsilon}\right)\frac{\partial\varepsilon}{\partial x_j}\right]+\frac{\varepsilon}{k}(C_{\varepsilon 1}P_k-C_{\varepsilon 2}\rho\varepsilon) \quad (9),$$

where k is the turbulent kinetic energy, ε is the turbulent kinetic energy dissipation rate, P_k represents the generation of turbulent kinetic energy due to the mean velocity gradients, σ_k, σ_ε, $C_{\varepsilon 1}$ and $C_{\varepsilon 2}$ are model coefficients. The numerical model uses a finite volumes, coupled implicit, pressure based solution technique. A high-resolution differentiating scheme was used, which locally adjusts the discretisation to be as close to Second-Order as possible, while ensuring boundedness of the solution.

2.1. Simulation

In the numerical study of the vacuum cleaner unit, a steady state approach was used with a single rotating frame of reference. A stage interface was used between rotating impeller and both steady inlet region and diffuser. Stage interface is modeled using a mixing plane – flow quantities are averaged in the pitch wise direction through the mixing plane, whereas their actual distribution is maintained in axial direction. An unstructured tetrahedral mesh was used with hexahedral layer mesh at the wall boundaries. The analysis was carried out through the whole suction unit, including diffuser and motor part (Fig. 1). The overall mesh consisted of 477,149 nodes; one impeller blade passage was modeled with 30,070 nodes. A periodic boundary condition was used to model full geometry. A mesh sensitivity study was carried out to ensure that appropriate mesh density was chosen for the simulations. While finer mesh (640,178 nodes) did not show any considerable improvement in accuracy of flow quantities, coarser mesh (375,983 nodes) exceeded the predicted inlet pressure and air efficiency of vacuum cleaner unit by as much as 20%.

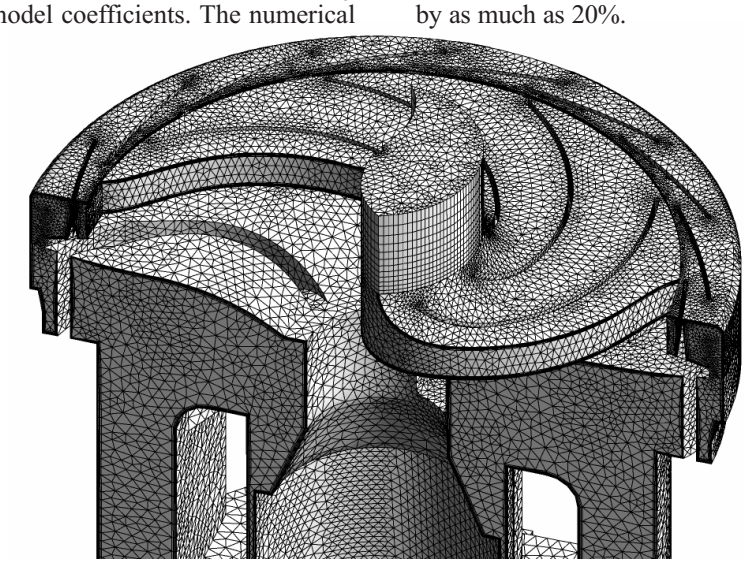

Fig. 1. *Mesh model of the impeller, diffuser, return channels and the electrical motor. Outlet region is not shown here.*

The walls were modeled as adiabatic smooth walls and the scalable wall functions were used as a boundary condition. Measured values of mass flow rate and static temperature were prescribed at the inlet, static pressure and temperature at the outlet. Outlet boundary condition was prescribed as an opening at the exhaust openings of motor housing.

Two sets of simulations were carried out using air as a compressible and incompressible working fluids. In the compressible case, we used air as an ideal gas and in the incompressible case we used air with constant properties at 25 °C. Of the whole volume flow / pressure characteristics curve of the suction unit, we analyzed two operating points that match the measurement points of the experiment. Numerical results for both selected volume flows show very good agreement with the pressure/volume flow characteristics of the suction unit with discrepancy of inlet pressure and aerodynamic efficiency values being within 4%. Residual target of 10^{-4} was achieved in converging calculations, usually within 300 iterations.

3 EXPERIMENTAL SETUP

3.1 Test Rig

Measurements were conducted on a shrouded impeller with nine 2D blades (Fig. 2). The cover of the vacuum cleaner unit and the shroud of the impeller were manufactured from perspex, which enabled us to follow the particles through the entire impeller channel.

Impeller was submerged in the test rig as shown in Figure 3. A glass tank was used with dimensions 400x400x350 mm. The flow medium was circulating inside the test rig so that working conditions were constant. Testing impeller was operating inside the original vacuum cleaner unit, driven by external asynchronous motor. Asynchronous motor was controlled by a frequency regulator.

Seeding particles with radius of 0.5mm were made out of polypropylene to have the same density as working medium. Particles were introduced into the impeller at radius R_0=0 mm. For visualization we used non-interlaced CCD camera Sony XC HR-50. Resolution of the camera was 640x480 pixels, which equals 140x105 mm. Sampling frequency is f_s=60 Hz and exposure time is $t = 5 \cdot 10^{-4}$ s. Camera was positioned under a glass tank in the axis of the impeller. For illumination we used ring illuminator Vega Velum DC. With appropriate positioning of the illumination source and the camera, the reflections of light were reduced to a minimum. The images were digitized and recorded using a frame grabber NI 1409 and a NI Vision software module running on a Labview software platform.

Temperature was measured using Pt-100 resistance thermometer and maintained in the liquid vessel at the temperature region ±1°C.

3.2 Selection of Measurement Point

Figure 4 shows pressure/volume flow characteristics curve of the vacuum cleaner suction unit under operation with air. Measurements with water were conducted in dynamically equivalent points at high volume flow Q_1=1.46Q_n, n_1 =336.8 rpm (measurement point 1) and nominal flow Q_2=Q_n, n_2 =359.5 rpm (measurement point 2).

Measurement points 1 and 2 were obtained by setting the rotational speeds which were calculated

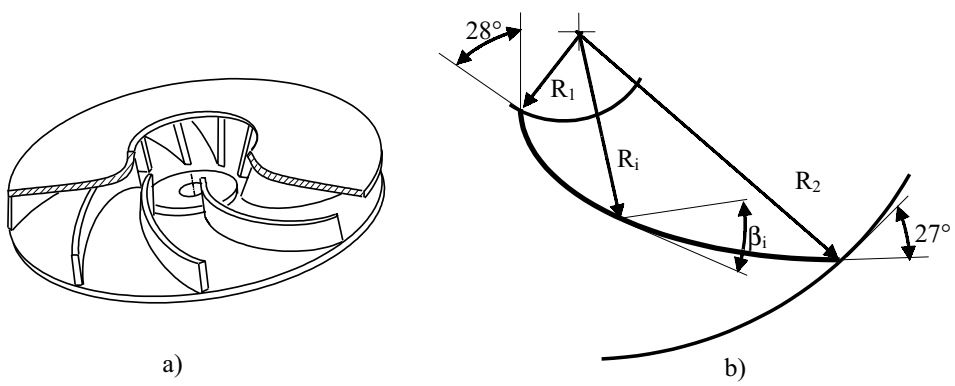

Fig. 2. *Geometry of the centrifugal impeller; a) impeller 3D cross section and b) impeller blade angles*

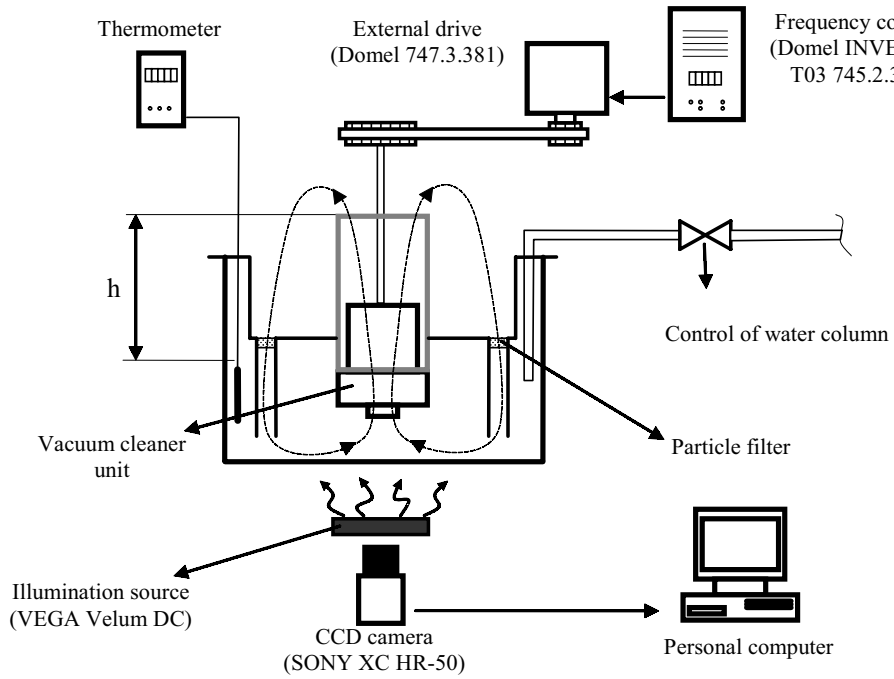

Fig. 3. *Closed loop test rig*

in accordance with Equation 4 and by setting appropriate water column height that corresponded to selected static pressure. Both measurement points are on the same pressure/volume flow characteristics.

The sampling frequency of the camera and the dimensions of the test rig were considered when selecting the pressure/volume flow characteristics. Thus, we were able to record sufficient number of consecutive images of the same particle at high volume flow, and the height of the water column was kept moderate at high pressures (nominal volume flow).

In each of the two measurement points, we conducted 15 measurements and for each of the measurement we recorded a series of 200 consecutive images.

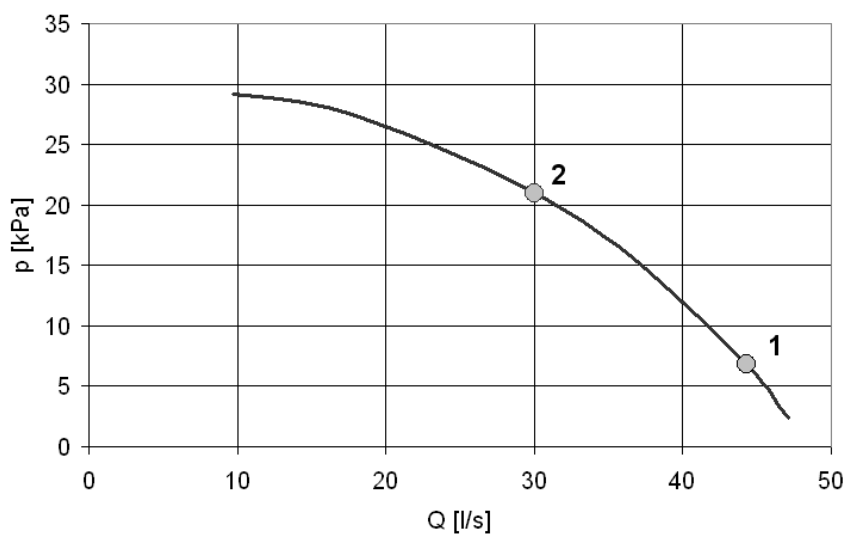

Fig. 4. *Pressure/volume flow characteristics curve of the vacuum cleaner suction unit under operation with air. Dots show measurement point at a high volume flow $Q_1=1.46Q_n$ (measurement point 1) and at nominal flow $Q_2=Q_n$ (measurement point 2).*

3.3 Image Analysis

The purpose of image analysis was to establish occurrences of particles in the centrifugal rotor.

For the purposes of the analysis, a computer program called TRACER was written in C++. Tracer enabled to rotate pictures in correlation with impeller revolutions. This enabled to follow the particle through the seemingly static impeller blade channels. Furthermore, this feature also enabled to make a computing corrections of the impeller frequency, which was varying during the measurements within the range of 1 Hz.

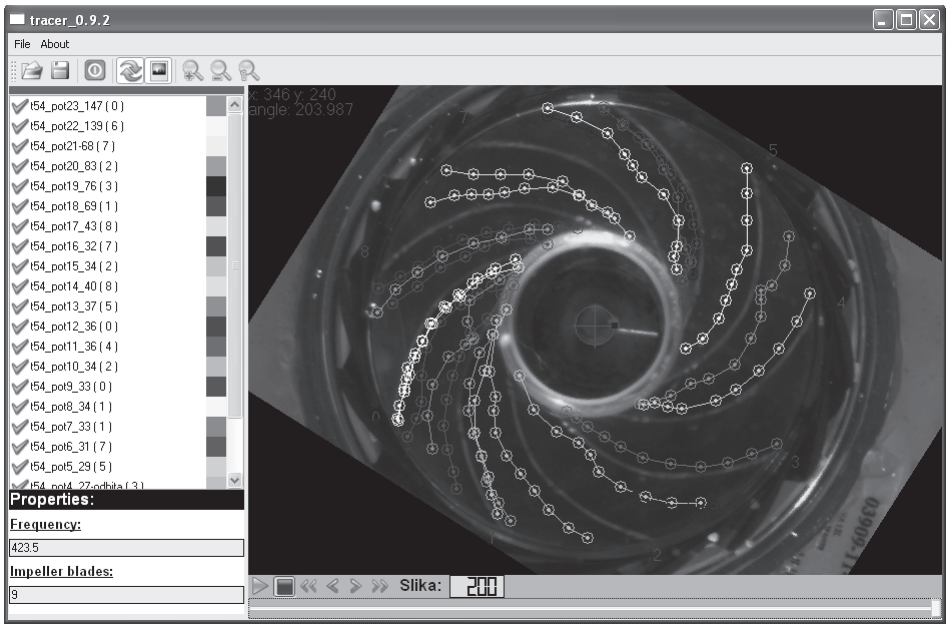

Fig. 5. *Trajectories of a single measurement at nominal volume flow*

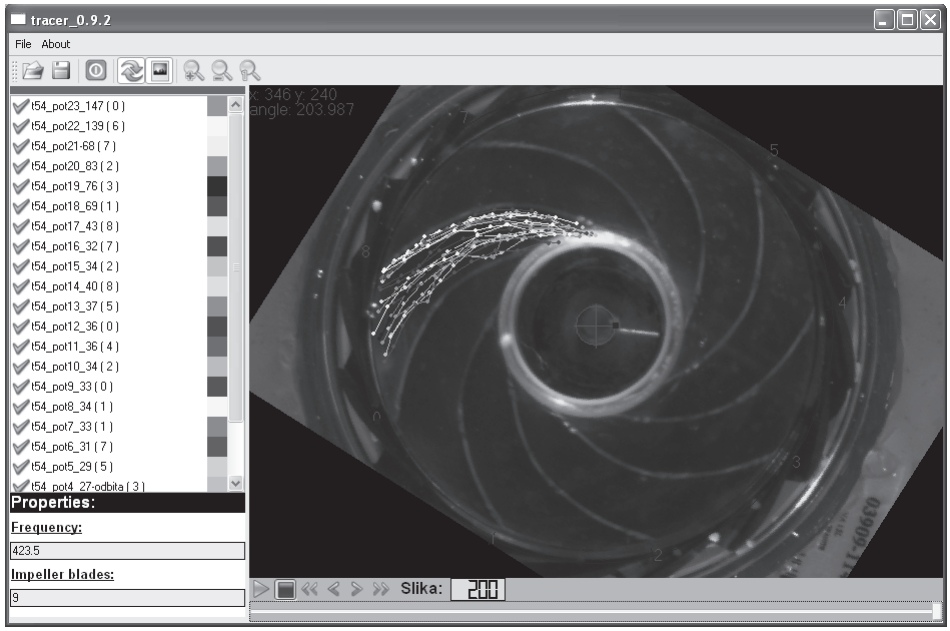

Fig. 6. *Trajectories of a single measurement at nominal flow after the rotation into a single blade channel*

Measurement error due to changing frequency was already reported in reference [1], where its influence was much greater because of the longer measuring time.

On average, we captured 16 trajectories per measurement and the measurement itself lasted 3.3 secs. Trajectories were captured through different impeller blade channels (Fig. 5). Occurrences of particles were defined with accuracy of 1 pixel which equals 0.22 mm. Trajectories were further rotated into a single impeller blade channel (Fig. 6).

4 RESULTS OF MEASUREMENTS AND COMPARISON WITH CFD SIMULATIONS

Results of experimental measurements are based on image analysis, performed with the TRACER program. From the established occurrences of the particles we were able to define trajectories of a single particle and its relative velocity. Altogether, 246 trajectories were captured at measurement point 1 and 199 trajectories were captured at measurement point 2.

4.1 Trajectories

4.1.1 Experimental Results

At each flow rate, 15 measurements were conducted and for each measurement, an average trajectory was calculated. In this way, we got 15 average trajectories in each of the two measurement points. To calculate average trajectory, we divided the length of the channel into several sections. The number of the sections equals the lowest number of detected occurrences of particles of individual trajectory in the measurement. If one trajectory had several occurrences in one section an average location of this particle in the observed section was calculated. In this way, particles with lower relative velocity do not have greater influence on average trajectory than particles with higher relative velocity, which have consecutively lower number of occurrences of particles.

Envelopes of average trajectories are shown in Figures 7 and 8. Hatched areas indicate region of occurrence of average trajectories.

It can be seen that average trajectories move from the pressure side towards the suction side of the impeller blade channel when moving from high flow at measurement point 1 (Fig. 7) towards the nominal volume flow at measurement point 2 (Fig. 8).

Comparison between the average trajectory of particles in each of the measuring points and the blade curvature is shown in Figure 9. Tangential angles of average trajectories and of the impeller blades are given in table 1. Angles were measured at radii 22, 28, 34 and 40 mm. The relative flow angles were not determined at inlet and at outlet of the channel. The reason for this is the method of measurement, which enables determining trajectories from occurrences of particles on visualization images. Because the acquisition frequency of the camera was limited to 60 Hz, images with occurrences of particles at the inlet and outlet were seldom available. From Figure 9 we can notice congruence between the average trajectory at nominal flow and the impeller blade. Average trajectory at large flow is more back swept

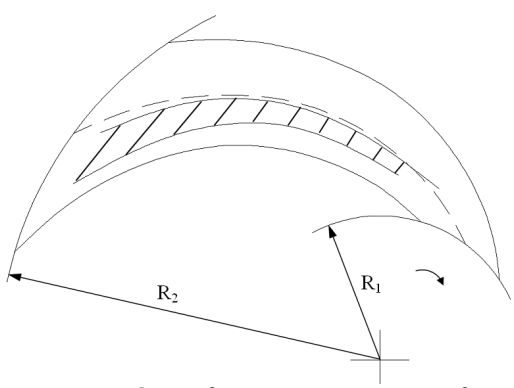

Fig. 7. *Envelope of average trajectories of 15 measurements at $Q_1=1.46Q_n$ in n_1 =336.8 rpm. Dashed line indicates the middle line of the blade channel.*

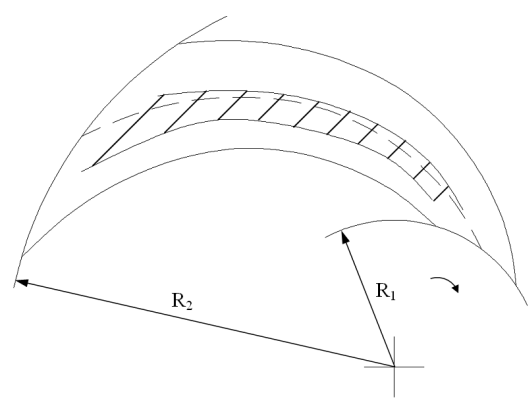

Fig. 8. *Envelope of average trajectories of 15 measurements at $Q_2=Q_n$ in n_2 =359.5 rpm. Dashed line indicates the middle line of the blade channel.*

Table 1. *Tangential angles of the average trajectories and the impeller blade at diferent radii*

	β [°] R=22mm	β [°] R=28mm	β [°] R=34mm	β [°] R=40mm
Impeller blade	33.4	34.7	29.9	28.4
Average trajectory in measurement point 1	25.4	34.3	27.7	28.6
Average trajectory in measurement point 2	35.5	31.1	32.4	27.8

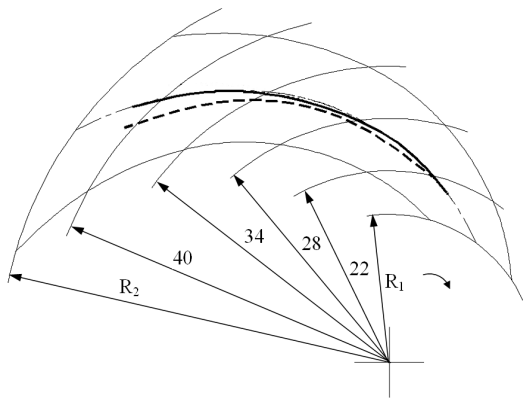

Fig. 9. *Average trajectory of particles at high flow Q_1=1.46Q_n (dashed line) and at nominal flow Q_2=Q_n (continuous line)*

in comparison to the impeller blades. Average trajectories also indicate negative incidence angle at nominal flow and positive incidence angle at high flow.

At both measurement points, we observed trajectories that indicate existence of turbulent flow. At nominal flow in measurement point 2, they represented 7% and at high flow at measurement point 1 they represented 3 % of all recorded trajectories. The reason for lower number of turbulent trajectories at high flow in comparison with nominal flow can also lie in the fact that we have lower number of captured occurrences of particles at high flow and thus less detailed trajectory can be drawn.

Figures 10 and 11 show four characteristic turbulent trajectories that occurred in each of the two measurement points. As we observe from Figures 10 and 11, trajectories at large and nominal flow detach from the pressure side of the blade, which indicates vortices that appear on the last two thirds of the blade. Observations also indicate that these vortices are not steady but they are appearing and disappearing with time.

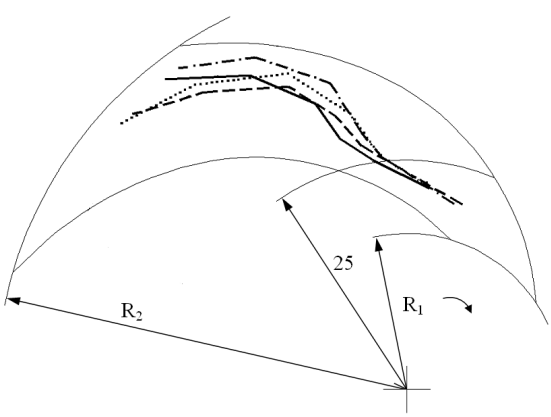

Fig. 10. *Trajectories that indicate turbulence at high flow Q_1=1.46Q_n*

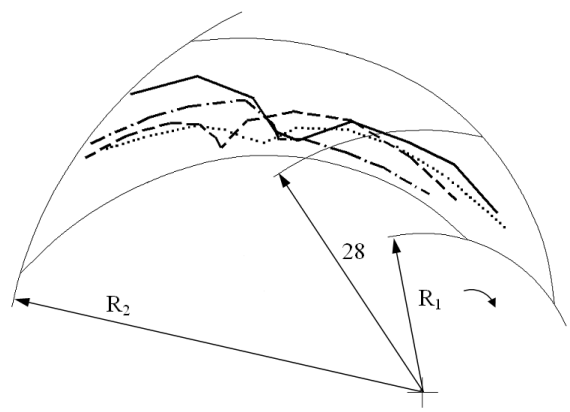

Fig. 11. *Trajectories that indicate turbulence at nominal flow Q_2=Q_n*

4.1.2 CFD Analysis

Numerically calculated streamlines for high and nominal flows are given in Figures 12 and 13. Numerical results when using compressible fluid (Figs. 12a and Fig. 13a) and when using incompressible fluid (Figs. 12b and 13b) show negligible differences when comparing streamline plots. However, there is an observable difference in the overall air efficiency of a vacuum cleaner unit. Difference in efficiency between measured and numerical results for compressible fluid was 3.72 % at nominal flow and 4.45% at high flow, while the difference in efficiency between measured and numerical results for incompressible fluid was 11.12% at nominal flow and 23.00% at high flow.

We can observe at experimental evaluation as well as at numerical simulation that there is detached fluid on the pressure side of the blade

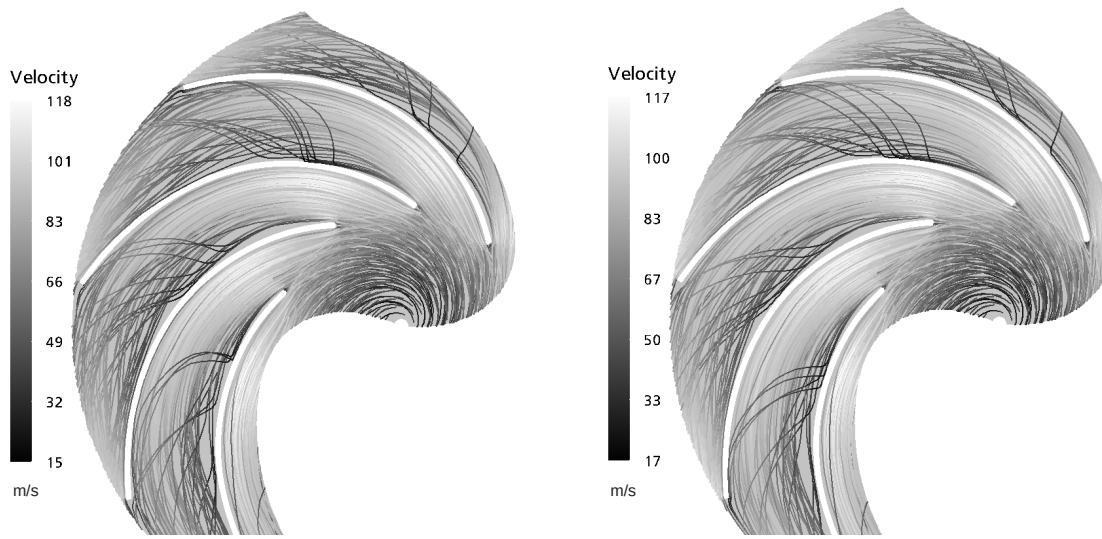

a) b)

Fig. 12. *Numerically calculated streamlines at high flow $Q_1=1.46Q_n$ using a) air as a compressible working fluid and b) air as an incompressible working fluid*

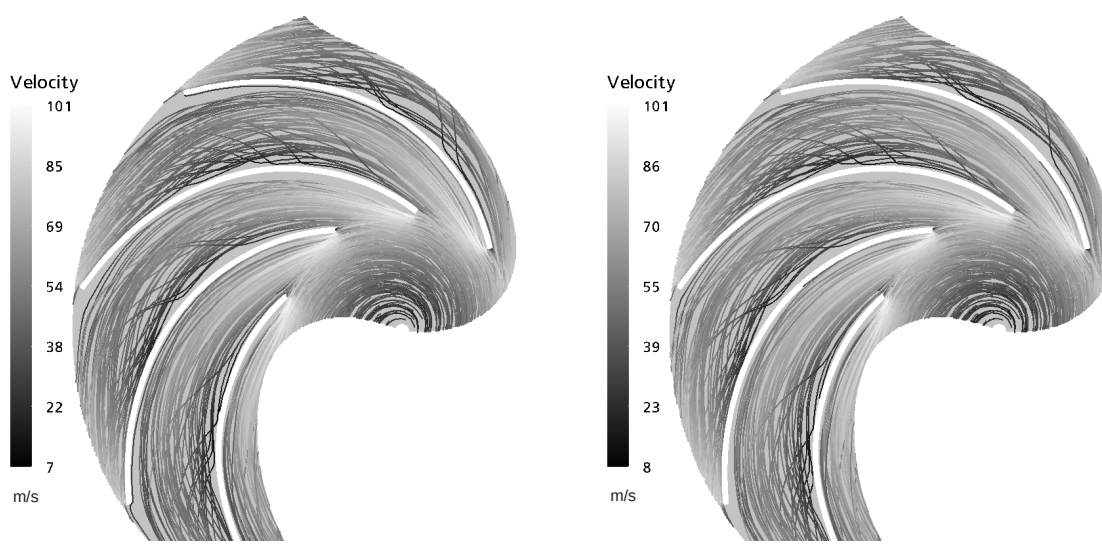

a) b)

Fig. 13. *Numerically calculated streamlines at nominal flow $Q_2=Q_n$ using a) air as a compressible working fluid and b) air as an incompressible working fluid*

channel. At both operational points experimental results agree with numerical results well.

4.2 Relative Velocity

By following the particles through impeller blade channels, we were able to calculate relative velocities. The path was determined with the distance between two successive occurrences of the particle and the time was determined by sampling frequency. When calculating relative velocities in this manner, one has to assume that velocity between two successive occurrences of particles is constant and that the flow through the impeller is two dimensional.

4.2.1 Experimental Results

From the experimental results, the velocities were estimated from two consecutive occurrences of the particles. The velocity was assigned to the middle point between both consecutive occurrences of particles. Due to this, the density of points with assigned velocity near the inlet and the outlet of the blade passage was low. This resulted in a lower accuracy of the inlet and outlet relative velocities (Figs. 14 and 15). The accuracy depends on the number of velocity points and this was not the same in all parts of the blade channel. The mesh in Figures 14 and 15 was calculated using the 9th order two dimensional polynomial regression. The results were calculated using Equations (1) to (5) from water to air as a medium to enable comparison with CFD results.

Figure 14 shows relative velocities at high volume flow. The relative velocity at the inlet channel is higher on the suction side of the blade. This region extends to approximately one third of the blade length. Further to the outlet region near the suction side of the blade, the relative velocities are low and the peak of relative velocities shifts towards the center of the channel and to the pressure side. There are areas of small relative velocities near the pressure side of the blade channel and at the tip of the pressure side of the blade at the outlet. However, this could be due to the low number of data used for meshing in this region.

Figure 15 shows relative velocities at nominal volume flow. The most important feature is the presence of a region with low relative velocities at the suction side of the blade which extends from approximately one third of the blade to the outlet of the blade. At the inlet, the measured relative velocities are higher, although this could also be due to the low number of velocity points in this region. At the outlet of the channel, there are higher velocities on the pressure side of the blade. There is a region of low relative velocities in the middle of the pressure side, similarly to what happened to a smaller extent in the case of high volume flow (Fig. 14).

4.2.2 CFD Analysis

The relative velocities were calculated. Results are shown in Figures 16 and 17. Figure 16 shows relative velocities at a high volume flow. On the

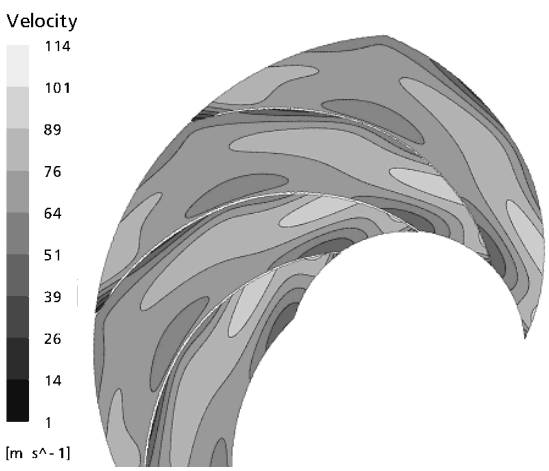

Fig. 14. *Relative velocities at high flow* $Q_1=1.46Q_n$

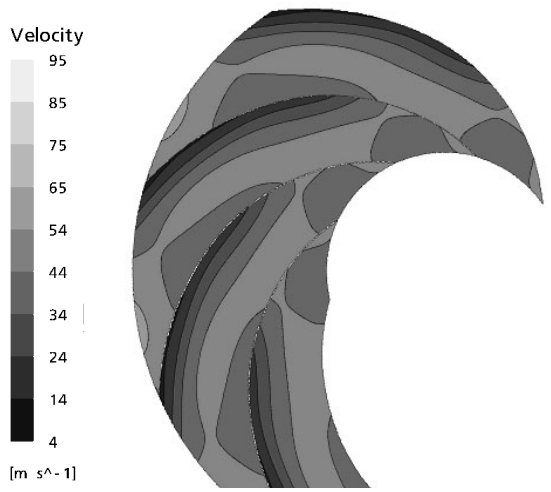

Fig. 15. *Relative velocities at nominal flow* $Q_2=Q_n$

pressure side of the blade there is a region of secondary flow with very low relative velocities, starting from the tip of the blade and extending to approximately two thirds of the blade length. The peak of relative velocities amplitude is located at approximately one fourth of the channel close to the suction side of the blade. The relative flow velocity at the outlet of the channel is low on its suction side and high on its pressure side. The maximum velocities exceed 100 m/s.

Figure 17 shows relative velocities at nominal volume flow. Here, the point of the highest velocity is close to the tip of the blade on its suction side. The position of the highest relative velocities

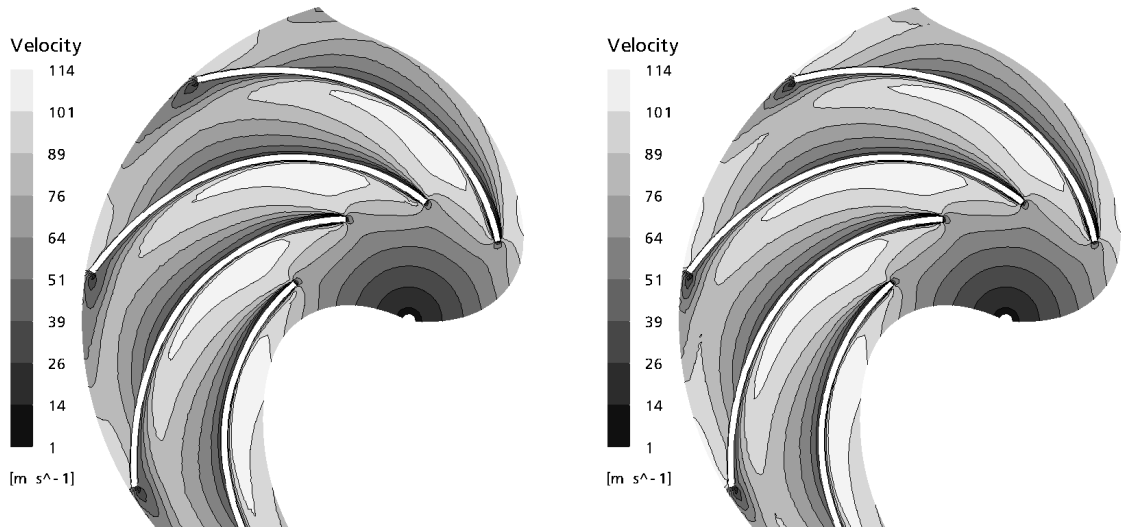

a) b)

Fig. 16. *Numerically calculated relative velocities at high flow $Q_1=1.46Q_n$ using a) air as a compressible working fluid and b) air as an incompressible working fluid. Plots show relative velocities at middle surface between the hub and the shroud.*

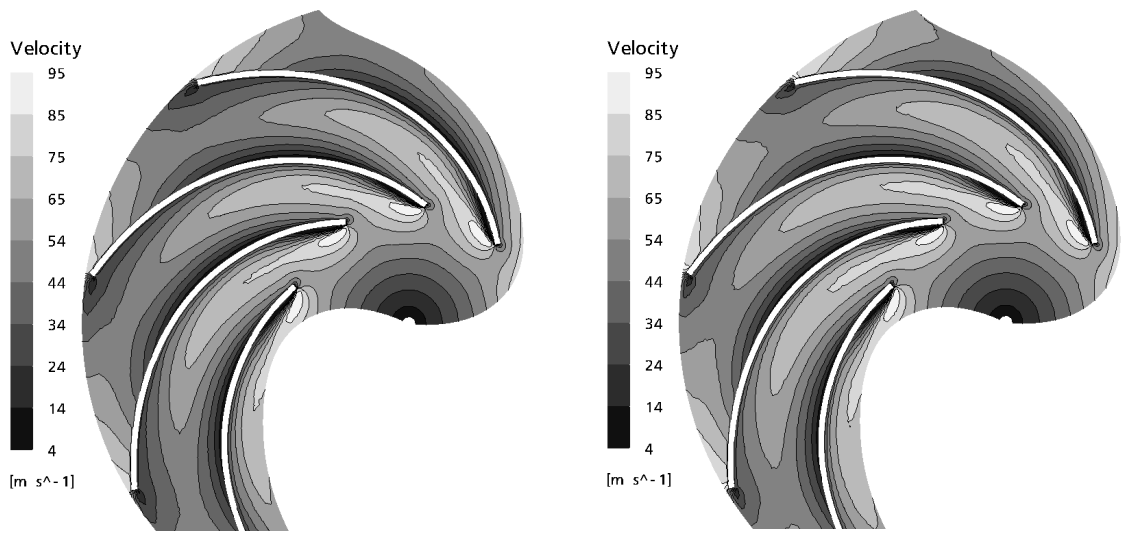

a) b)

Fig. 17. *Numerically calculated relative velocities at nominal flow $Q_2=Q_n$ using a) air as a compressible working fluid and b) air as an incompressible working fluid. Plots show relative velocities at middle surface between the hub and the shroud.*

has moved from the suction side to the center of the channel. The same phenomenon of the secondary flow at the pressure side of the blade and distribution of velocities at the outlet of the channel was established as in Figure 16. Maximum velocities exceed 85 m/s.

No significant differences in relative velocities amplitudes and distribution were established between compressible and incompressible flows. This supports the use of experimental technique based on incompressible water flow visualization.

Comparison between experimental results and numerical simulation shows good agreement between both methods. Using both methods, we observe a region of high relative velocities along the suction side of the blade located at approximately the same position. Both methods similarly predict a region of low relative velocities at the end of the blade at the suction side. We also notice a region of low relative velocities along the center of the pressure side of the blade and a region of high relative velocities at the outlet of the channel at the pressure side of the blade.

5 DISCUSSION

In the follow-up, we will discuss the above results and compare results of experimental work with results of CFD analysis.

Particle size and material selection is influenced by inertia, gravity and buoyancy forces of the particles. To ensure following of the particles to the flow, the selected density of particles matched the density of flow medium. The diameter of particles was dictated by the illumination technique. We used continuous illumination and thus, a relatively large size (radius r = 0.5mm) of particles was necessary, in contrast to the size of particles used in PIV methods [1]. Using the theory of similarity, influence of the inertia of particles was reduced by lowering the number of rotations.

The compressibility of air should be taken into account generally as Mach number increases to 0.3 or higher. In the current research, we achieved maximum velocities of up to Mach 0.6. By using water as a medium, we were not able to consider compressibility and we relied on the comparison between CFD results with compressible and non compressible flows. As shown in Figures 12, 13, 16 and 17, differences between both cases exist, but they are generally negligible. Although there was no significant difference between streamlines and relative velocities, there is a noticeable difference between the suction efficiencies of the two flows.

The flow is also influenced by the Reynolds number. In our case, the Reynolds number of the measurements in water was approximately 31% of the corresponding Reynolds number in air.

The relative velocities as a result of CFD analysis are shown in Figures 16 and 17. At both operational flows, we noticed that average relative velocities calculated using CFD method are on the average a little higher than the corresponding measured velocities shown in Figures 14 and 15. In our opinion, the main reason for this is the selection of the plane where relative velocities are shown. This was at the center of the channel for the CFD, while in case of experimental techniques; velocity of particles was averaged over the entire width of the impeller flow channel.

A comparison with CFD showed that the presented experimental method enables measurements of flow properties inside the impeller with a reasonable accuracy.

These results indicate further possibilities for the changes of the geometry of the impeller to achieve better flow conditions.

6 CONCLUSION

Numerical simulation and flow visualization through the vacuum cleaner centrifugal impeller at nominal (Q_n) and at high flow ($1.46Q_n$) were compared.

Flow visualization was conducted with the use of the theory of dynamical similarity where experimental flow medium was water. The experiment confirmed good matching between the calculated and measured values for pressure difference, rotational speed and volume flow, when using air as a flow medium and when using water as a flow medium.

Both experimental visualization and numerical simulation indicate detachment of the flow after one third of the blade length from the pressure side of the blade. Detachment occurs at high flow as well as at nominal flow. Average trajectory of the particle shows congruence with blade curvature at nominal flow, meanwhile the average trajectory at high flow is more back swept at trailing edge and has a positive incidence angle

at the leading edge. There is a good agreement in distribution of relative velocities between the pressure and the suction side of the channel obtained by experimental measurement and numerical simulation at a high flow. The similarity decreases when comparing distribution of relative velocities at nominal flow.

An advantage of such approach to experimental flow visualization is that it enables observing the flow in different operation conditions. Because it is possible to get numerical solutions for almost all operation conditions, it is necessarily to get also a confirmation of these results experimentally and thus gain the confidence in numerical computation. Although we achieved relatively good comparison of the results between experimental measurement and numerical simulations, one has to be aware that it is most often impossible to fulfill all conditions for dynamic similarity. The influence of conditions that are not fulfilled should be evaluated and considered when evaluating the final results.

There is also possibility of automation of the presented experimental method by capturing of the positions of the particles in the flow, which would give the results in real time. The practical value of such method would be recognized in cases where there are numerous changing flow conditions.

7 REFERENCES

[1] Pedersen, N., Jacobsen, C.B. PIV Investigation of the Internal Flow Structure in a Centrifugal Pump Impeller. *10th International Symposium on Applications of Laser Techniques to Fluid Mechanics*, Lisbon, 2000.

[2] Irabu, K., Tamazato, E., Teruya, I. Velocity measurements of flow around a volute tongue of vaneless radial diffuser. *Proc. 3rd Asian Symposium on Visualization*, Japan, 1994.

[3] Širok, B., Grabec, I. Chaotis properties of a pulsating two-phase solid particles/gas flow. *Strojniški vestnik – Journal of Mechanical Engineering*, 34 (1988), p. 162-165. (In Slovenian).

[4] Novak, M., Širok, B., Hočevar, M., Oberdank, K. Simultaneous measurement of velocity fluctations and smoke tracer fluctations of turbulent flow over a back-facing step. *Journal of Flow Visualization and Image Processing*, vol 6., 1999, p. 221-229.

[5] Dular, M., Bachert, R., Širok, B., Stoffel, B. Transient simulation, visualisation and PIV-LIF measurements of the cavitation on different hydrofoil configurations. *Strojniški vestnik – Journal of Mechanical Engineering*, 51 (2005), p. 132-145.

[6] Lazarkiewicz, S., Troskolanski, T., A. *Impeller pumps*. Pergamon Press, Warszawa: Wydawnictwa naukowo-techniczne, 1965.

[7] *ISO 60193, Hydraulic turbines, storage pumps and pump turbines - Model acceptance tests*, IEC 60193 (1999-11).

[8] Bleier, P.F. *Fan handbook, selection, application and design*. New York: McGraw – Hill, 1998.

[9] Ferziger J. H., Perić M. *Computational Methods for Fluid Dynamics*, 2nd ed. Springer Verlag, 1999.

[10] Davidson, P.A. *Turbulence, an introduction for scientists and engineers*. New York: Oxford University Press, 2004.